Received: 2 March 2018 | Revised and accepted: 20 April 2018

DOI: 10.1002/wcms.1372

WILEY WIREs COMPUTATIONAL MOLECULAR SCIENCE

ADVANCED REVIEW

Microkinetic modeling in homogeneous catalysis

Maria Besora[1] | Feliu Maseras[1,2]

[1]Institute of Chemical Research of Catalonia (ICIQ), Barcelona Institute of Science and Technology, Barcelona, Spain

[2]Departament de Química, Universitat Autònoma de Barcelona (UAB), Barcelona, Spain

Correspondence
Feliu Maseras, Institute of Chemical Research of Catalonia (ICIQ), Barcelona Institute of Science and Technology, Avgda. Països Catalans 16, 43007 Tarragona, Catalonia, Spain.
Email: fmaseras@iciq.es

Funding information
CERCA Programme; Severo Ochoa Excellence Accreditation 2014–2018, Grant/Award Number: SEV-2013-0319; MINECO, Grant/Award Number: CTQ2017-87792-R

Computational homogeneous catalysis has focused traditionally on the calculation of free energy barriers, which are ultimately related to rate constants. Experiments do not focus on rate constants, but on reaction rates, which depend also on concentrations. The increasing efficiency of DFT and other electronic structure techniques has led to the development of models that provide quite accurate rate constants, to the extent that improved agreement with experiment requires the introduction of the role of concentration. Microkinetic modeling, consisting in the construction of explicit kinetic reaction networks merging the rate constants provided by calculation and concentration data supplied by experiment, is a simple and elegant way to introduce concentration effects in the computational description of homogeneous catalysis. It has a long history of application in computational heterogeneous catalysis and experimental biochemistry, but its use in computational homogeneous catalysis is still in an early stage. There are a number of situations in homogeneous catalysis where microkinetics have been shown to be critical, such as systems with complex reaction networks and systems where one key species has a concentration orders of magnitude different from the others. Microkinetic modeling, with its low computational cost, is likely to become a standard tool in computational homogeneous catalysis. It is certainly not necessary for all theoretical studies, but the researcher should always be aware of its existence.

This article is categorized under:
Structure and Mechanism > Reaction Mechanisms and Catalysis

KEYWORDS
DFT calculations, homogeneous catalysis, microkinetic modeling

1 | INTRODUCTION

Computational homogeneous catalysis is nowadays a mature field, as proved by the routine application of calculations to the achievement of a mechanistic understandings of many processes (Sameera & Maseras, 2012; Santoro, Kalek, Huang, & Himo, 2016; Sperger, Fisher, & Schoenebeck, 2016; Thiel, 2014). The main challenge for the computational chemist is often the characterization of a mechanism through the geometry optimization of intermediates and transition states. Afterward, most of the practical interpretations rely on the direct analysis of the free energy profiles. Barriers below 20 kcal/mol are considered synonymous with fast processes at room temperature, and values up to 30 kcal/mol have been deemed acceptable for reactions under heating. Comparison between the barriers for competing processes leads to estimation of selectivity ratios, where the case for enantioselective processes has been particularly successful (Balcells & Maseras, 2007; Hopmann, 2015).

Experiments do not measure directly free energy differences but the evolution of concentrations through time. These are ruled of course by chemical kinetics, where free energy differences, directly connected to rate constants, play indeed a key role. But this role is not exclusive, as concentrations are also important. This can be illustrated very easily with a simple

example: two competing second-order processes $R_0 + R_1 \rightarrow P_1$ and $R_0 + R_2 \rightarrow P_2$ taking place in solution. Their kinetic equations are $d[P_1]/dt = k_1[R_0][R_1]$ and $d[P_2]/dt = k_2[R_0][R_2]$. The rate of each reaction will depend on the corresponding reaction rate constant (k_1 or k_2) but also on the concentration of the involved reactants ($[R_1]$ or $[R_2]$). If the concentrations are similar the constants will decide it. But if they are not, and $k_1 \simeq k_2$, concentration effects will rule the selectivity. And concentration effects are conspicuously absent from standard free energy profiles.

A simple and elegant method for the introduction of concentration effects in the description provided by the free energy profiles is the use of microkinetic models. The basis of microkinetic modeling is fairly simple. A reaction network has to be built with all relevant elementary steps, and a reaction rate has to be assigned to each of them. This defines a system of differential equations, which can be solved numerically by using the initial concentrations of all the compounds as starting conditions. The microkinetic model will then provide an evolution of the concentration of each of the species through time, which is precisely what most experiments measure. The procedure has a moderate computational cost in most practical cases, as very simple arithmetic operations are involved. The use of microkinetic modeling is widespread in computational heterogeneous catalysis (Bligaard et al., 2004; Dumesic, Rudd, Aparicio, Rekoske, & Treviño, 1993; Mao, Wang, & Hu, 2017) and experimental biology (Herrgard et al., 2008; Slusarczyk, Lin, & Weiss, 2012; Trinh, Wlaschin, & Srienc, 2009). It has also been used in experimental homogeneous catalysis to test postulated mechanisms against experimental observations (Chmely et al., 2013; Colby, Bergman, & Ellman, 2008; Diao & Stahl, 2011; Miranda et al., 2013).

The use of microkinetic models has been so far rather scarce in computational homogeneous catalysis, but some relevant examples have been published. They were applied by Harvey and coworkers to a cobalt-catalyzed alkene hydroformylation (Rush, Pringle, & Harvey, 2014) and by Clot and coworkers to the activation of C—H bonds by palladium catalysts (Kefalidis, Davi, Holstein, Clot, & Baudoin, 2014). Aullón et al. (2015) used microkinetic models in the study on the competitive formation of different platinacycles. More recently, Jover (2017) applied them in the copper-mediated pentafluoroethylation of benzoic acid chlorides, Kalek and Himo (2017) in a cooperative process involving Meyer–Schuster rearrangement and Tsuji–Trost allylic substitution, Jaraíz et al. (2017) in the catalytic opening of epoxides by titanocene and Wei, Roisnel, Darcel, Clot, and Sortais (2017) in the hydrogenation of carbonyl derivatives by Rh catalysts. We have also experience in our group in the application of microkinetic modeling of computational homogeneous catalysis. We have used this treatment for the acceleration of the 1,3-dipolar cycloaddition inside cucurbit[6]uril (Goehry, Besora, & Maseras, 2015), in a photo-initiated aromatic perfluoroalkylation (Fernández-Álvarez, Nappi, Melchiorre, & Maseras, 2015), in the reaction of aryl halides with Ni-catalysts (Funes-Ardoiz, Nelson, & Maseras, 2017), and in a Pd-catalyzed decarboxylative C—C bond formation (Guo, Kuniyil, Gómez, Maseras, & Kleij, 2018).

The current review presents the results of the application of microkinetic modeling to a selected set of examples in computational homogeneous catalysis. The focus is placed on cases where numerical integration is applied to the rate equations in the reaction network obtained from calculation. Other approaches to microkinetic modeling, such as the use of the steady-state approximation are also possible. Most of the examples reported are taken from our work, and they have been chosen to highlight the contributions of microkinetic modeling to the chemical understanding of the processes, with the hope of extending its use in our research community.

We are aware that there are other valuable approaches to complement or refine the information extracted from free energy profiles, but they are beyond the scope of the current review. This is the case of standard state corrections from ideal gas to other conditions (typically 1 Molar), or the possible modifications to entropic corrections in the calculation of free energies in solution (Besora, Vidossich, Lledós, Ujaque, & Maseras, 2018). Microkinetic modeling is not directly connected either to refinements to transition state theory (TST) where the energy distribution between normal modes is not standard (Carpenter, Harvey, & Orr-Ewing, 2016; Fructos et al., 2017). The energy span model (Kozuch & Shaik, 2011) is on the other hand a treatment for catalytic processes that can be applied in cases where microkinetic modeling is not necessary. There is finally current research on methods for the automated generation of reaction networks (Dewyer, Arguelles, & Zimmerman, 2018; Martinez-Nuñez, 2015; Sameera, Maeda, & Morokuma, 2016) or extraction of information from their analysis (Kim, Kim, Kim, & Kim, 2018) that is not discussed here either.

2 | THE BASICS

2.1 | From $\Delta G^{\ddagger}$ to k

Kinetic experiments measure the change in concentrations with time, and from there, they obtain reaction rates. The macroscopic expression for the rate of a reaction $n_aA + n_bB \rightleftharpoons n_cC + n_dD$ is an expression of the form shown in Equation (1):

$$\text{rate} = \frac{1}{n_c}\frac{d[C]}{dt} = \frac{1}{n_d}\frac{d[D]}{dt} = -\frac{1}{n_a}\frac{d[A]}{dt} = -\frac{1}{n_b}\frac{d[B]}{dt} = k_{\text{forward}}[A]^{n_a}[B]^{n_b} \quad (1)$$

Care must be taken not to confuse equilibrium constant expressions with rate law expressions, although they are related as stated in Equation (2), where $\Delta G = \Delta G^{\ddagger}_{\text{forward}} - \Delta G^{\ddagger}_{\text{reverse}}$:

$$K_{\text{eq}} = \frac{[C]^{n_c}[D]^{n_d}}{[A]^{n_a}[B]^{n_b}} = \frac{k_{\text{forward}}}{k_{\text{reverse}}} = \exp\left(\frac{-\Delta G}{RT}\right) \quad (2)$$

The natural magnitude for computational kinetics is $\Delta G^{\ddagger}$, the free energy barrier measured as the energy difference between an intermediate and a transition state. Luckily, the relationship between $\Delta G^{\ddagger}$ and rate constant within the TST has been known since the 1930s, and is defined by the Eyring–Polanyi equation, see Equation (3) (Eyring, 1935):

$$k = \frac{\kappa k_{\text{B}} T}{h}\exp\left(\frac{-\Delta G^{\ddagger}}{RT}\right) \quad (3)$$

where k is the reaction rate constant, κ is the transmission factor, k_{B} is the Boltzmann's constant, T is the temperature, h is the Planck's constant, $\Delta G^{\ddagger}$ is the activation free energy, and R is the ideal gas constant. The transmission factor κ is assumed to be 1 in most practical cases in homogeneous catalysis. The reaction rate has dimensions of concentration per unit of time, the dimensions of k depend thus on the exponents of the concentration terms in the rate law, the reaction order. It follows thus that, for reactions with order different from 0, the specific value of the rate constant will depend on the reference state. Another nuance is that taking a different species as origin of energies, the $\Delta G^{\ddagger}$ will change, will change the reaction equation and so the reaction rate constant. It is important to notice that if the definitions are consistent, identical concentration evolutions can be reached from different reference states or origins of energies.

2.2 | From k to microkinetic model

The large majority of processes in homogeneous catalysis involve multiple steps. These may include off-cycle formation of the catalyst from a pre-catalyst, formation of adducts between the reactants, catalyst deactivation processes, interactions between the reactants, reactive steps where bonds are formed and broken, isomerizations, etc. Each of the steps has a reaction rate constant and contributes with more or lesser extend to the kinetics of the process. The kinetic model puts all these processes together.

We will see with a generic example how a microkinetic model would work for a simple catalytic process. In Figure 1 we have set a simple catalytic cycle. The catalyst reacts with react1 to form adduct INT1, INT1 incorporates react2 to form INT2, which evolves to intermediate INT3. INT3 then releases the product prod and recovers the catalyst.

Once all chemical equations are written down as depicted in Figure 1, the kinetic equations can be formulated, as shown in Figure 2. The idea here is to take into account all the processes leading to the formation or consumption of each single species in the system. All forward and reverse chemical equations have to be considered. This defines a system of differential equations, where the rate constants can be obtained from the free energy profile by converting $\Delta G^{\ddagger}$ values to rate constants following the expression in Equation (3). The system of differential equations in Figure 2 must then be solved introducing the initial concentrations of each species as limit conditions. This solution may be analytical (in the simpler cases) or numerical. Other alternative resolutions are also possible and might be convenient to reproduce some experimental data such as the popular steady-state approximation. A computational code may be written for the solution, although useful software is freely available for this purpose, see Section 4 for further details. The solution of the differential equations provides the evolution of the concentrations of all participating species over time.

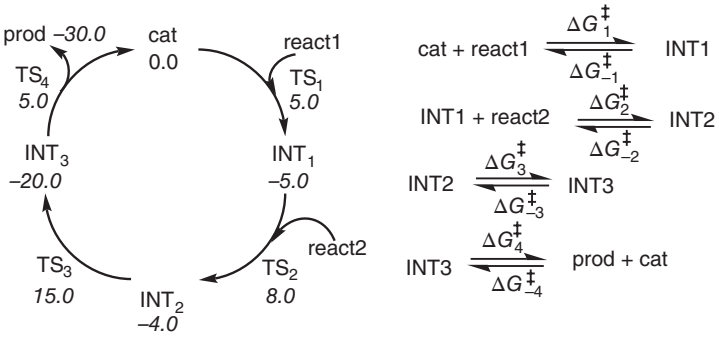

FIGURE 1 Example of catalytic cycle with corresponding chemical equations and associated free energies for each species. Energies in kcal/mol

Kinetic equations

$$\frac{d[cat]}{dt} = -k_1[cat][react1] + k_{-1}[INT_1] + k_4[INT_3] - k_{-4}[cat][prod]$$

$$\frac{d[INT1]}{dt} = k_1[cat][react1] - k_{-1}[INT_1] - k_2[INT_1][react2] + k_{-2}[INT_2]$$

$$\frac{d[INTz]}{dt} = k_2[INT_1][react2] - k_{-2}[INT_2] - k_3[INT_2] + k_{-3}[INT_3]$$

$$\frac{d[INT3]}{dt} = k_3[INT_2] - k_{-2}[INT_3] - k_4[INT_3] + k_{-4}[prod][cat]$$

$$\frac{d[reactI]}{dt} = -k_1[cat][react1] + k_{-1}[INT_1]$$

$$\frac{d[react2]}{dt} = -k_2[INT_1][react2] + k_{-2}[INT_2]$$

$$\frac{d[prod]}{dt} = k_4[INT_3] - k_{-4}[prod][cat]$$

Initial conditions

$[cat]_0 = 0.2$ M

$[react1]_0 = 0.6$ M

$[react2]_0 = 0.5$ M

$[prod]_0 = [INT_1]_0 = [INT_2]_0 = [INT_3]_0 = 0.0$

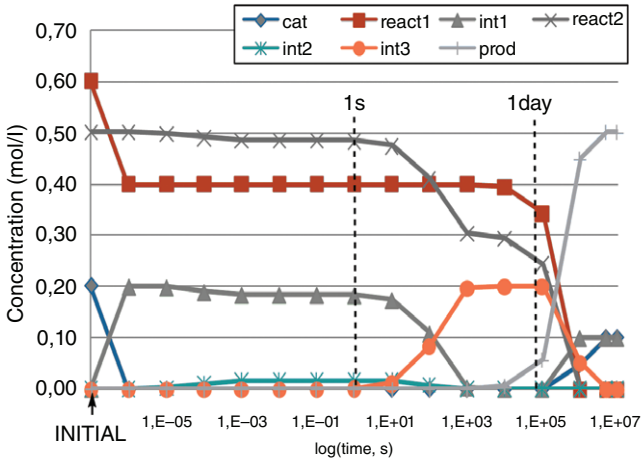

FIGURE 2 Differential equations derived from the example catalytic cycle depicted in Figure 1 and initial concentrations. A graphic with the microkinetic model outcome with concentrations of the species involved in the example (mol/L) over time (time in logarithmic scale and in seconds) is also presented

We can analyze the behavior of our generic system by looking at the plot in Figure 2. The concentration of INT1 increases as the reaction starts, but at about 10 s decreases sharply and INT3 is formed instead. INT3 is the dominant species between 10^2 and 10^5 s. It starts decreasing after 10^5 s to form the final product. INT1 is formed again when react2 is fully consumed (and the reaction finished) with the react1 in excess. There is an additional excess of 0.1 M of catalyst, which remains as such.

The qualitative behavior for the system above can certainly be predicted without the microkinetic model. The rate limiting step is the product release from INT3, with a barrier of 25 kcal/mol (from INT3 to TS4). The magnitude of this barrier is consistent with the reaction time observed in the plot for the formation of the product. Not all practical systems are so easy to predict from inspection of the free energy profile, as we will see in the following sections.

3 | CASE EXAMPLES

3.1 | Concentration effects without microkinetic modeling

Microkinetic modeling is an elegant way for the introduction of concentration effects in computational homogeneous catalysis. Its application is relatively recent, but the importance of concentration effects had been previously recognized by several authors, which introduced them in a variety of ways. We review here some of these applications, which may be viewed as implicit microkinetic modeling (Jensen, Koley, Jagadeesh, & Thiel, 2005; Muñoz-Molina et al., 2011).

Cramer and coworkers observed the importance of taking into account the correct concentration of protons when studying acid/base reactions. They designed a treatment (Kelly, Cramer, & Truhlar, 2006), which then applied to a variety of reactions such as reduction of nitroaromatic compounds (Hartenbach et al., 2008), copper-catalyzed water oxidation (Winikoff & Cramer, 2014), and the electrochemical reduction of dinitrotoluene (Olson, Isley, Brennan, Cramer, & Buehlmann, 2015). The idea is to use as reference state for proton/hydronium concentration that corresponding to the real pH in the reaction. There is thus a correction of −7.7 kcal/mol when moving from pH = 1 to pH = 7. In this way, it can be shown how prohibitive processes in acid conditions can become feasible in basic conditions, and vice versa. This type of correction works very well for buffered systems, but does not allow taking into account changes in the concentration along the reaction. The so-called stochastic simulations by Michalak and Ziegler (2002, 2003) on the competition between propagation/branching/termination in olefin polymerization processes can also be viewed as a variation of microkinetic modeling.

We discuss in detail here one example from our work on the activation of C—H bonds by metallocarbene complexes. We have studied throughout the years a number of these reactions, in most cases without need for microkinetic models (Besora et al., 2015; Corro et al., 2014; Fructos et al., 2017; Gava et al., 2014). A notable exception is the competition between alkane

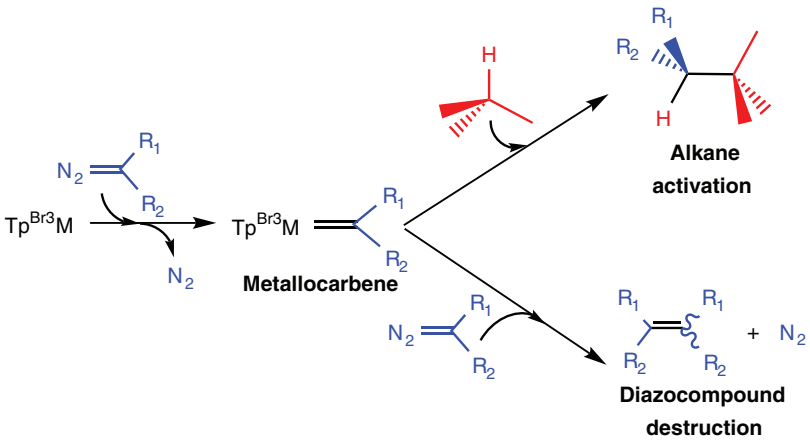

FIGURE 3 Schematic representation of the competition between alkane activation and diazocompound destruction (homocoupling) processes

activation and diazocompound destruction by a homocoupling reaction with a diazocompound (Braga et al., 2011), see Figure 3. The diazocompounds are used in the generation of the catalyst from a precursor, and must be thus present in the reaction media, which poses a potential problem for the efficiency of the system. The free energy barriers for both processes were computed for two different metallocarbene complexes, one with silver and another with copper. For silver, the barrier for alkane activation was found to be 12.5 kcal/mol, and that for diazocompound destruction was 9.2 kcal/mol. The corresponding values for copper were 16.6 and 9.9 kcal/mol, respectively. Direct inspection of the barriers suggested diazocompound destruction for both metals, as the energy differences between the competing transition states are well above 3 kcal/mol. This is not the experimental observation, and the result can be explained by taking into account concentration effects. Alkane is the solvent, thus in high concentration, and the diazocompound is in low concentration, but both compounds compete directly for reaction with the metallocarbene in the key step shown in Figure 3. We were able to discuss this result quantitatively by using Equation (4):

$$\frac{\nu_{\mathrm{DEST}}}{\nu_{\mathrm{CAT}}} = \frac{[\mathrm{diazo}]}{[\mathrm{alkane}]} \exp\left(-\frac{\Delta G^{\ddagger}_{\mathrm{CAT}} - \Delta G^{\ddagger}_{\mathrm{DEST}}}{RT} \right) \tag{4}$$

In this equation we estimate the ratio between reaction rates for the catalysis, ν_{CAT}, and diazocompound destruction, ν_{DEST}. It has two contributions: one depends on the concentrations and the other on the free energies. For silver complexes, the difference between the $\Delta G^{\ddagger}$ for the two processes is of 3.3 kcal/mol. This means that the concentration of alkane needs to be 263 times larger than that of diazocompound to get 50% of each product, and 2.6×10^4 times larger to achieve 99% of the insertion product. These numbers look high, but they correspond to the experimental conditions as the diazocompound is added in low concentrations while the alkane is used as solvent. For copper complexes, the difference in $\Delta G^{\ddagger}$ is 6.7 kcal/mol, much higher. In this case, the concentration of alkane needs to be 8.2×10^4 times larger for the two reactions to have the same rate (50% of each product), and 8.2×10^6 times larger to reach the 99%. This result agrees also with the experimental observation of significant diazocompound destruction even with very low concentration of diazocompounds.

3.2 | Large reaction networks

Microkinetic models are very helpful in the case of extended reaction networks where the more efficient reaction path is not obvious a priori. A representative example is supplied by our work on host–guest catalysis, in particular, on the acceleration of a 1,3-dipolar cycloaddition inside a cucurbit[6]uril supramolecule (Goehry et al., 2015). In this system, an azide, an alkyne, and the solvent compete for binding to the cucurbit[6]uril supramolecule. If one azide and one alkyne attach to the cucurbit[6]uril in the appropriate orientation they can form the triazole product. The complication is that there are multiple possible intermediates with fairly similar stabilities in solution and only one of them (**I**) leads to products, as depicted in Figure 4, left. The identification of the most abundant species in solution, which should be the origin for free energy barriers, is far from obvious. Microkinetic modeling was carried out to clarify the situation.

We will discuss the results of the evolution of species through time from the labels in Figure 4, right, where the free energies are also reported. The process starts with the reactants **A**, **B** and the macromolecular catalyst **E**. At the beginning of the reaction, **E** interacts mainly with the solvent to form species **O**. Then after the first nanoseconds, between 10^{-9} and 10^{-3} s, species **P** becomes the most relevant. It corresponds to the macromolecule containing a solvent molecule and a molecule of azide. After 10^{-3} s, **J**, a macromolecule containing only one alkyne, is the dominant species until it is overtaken at about 4 hr by species **N**, the product inside the cucurbit[6]uril. The practical free energy barrier for the reactivity of the system is thus

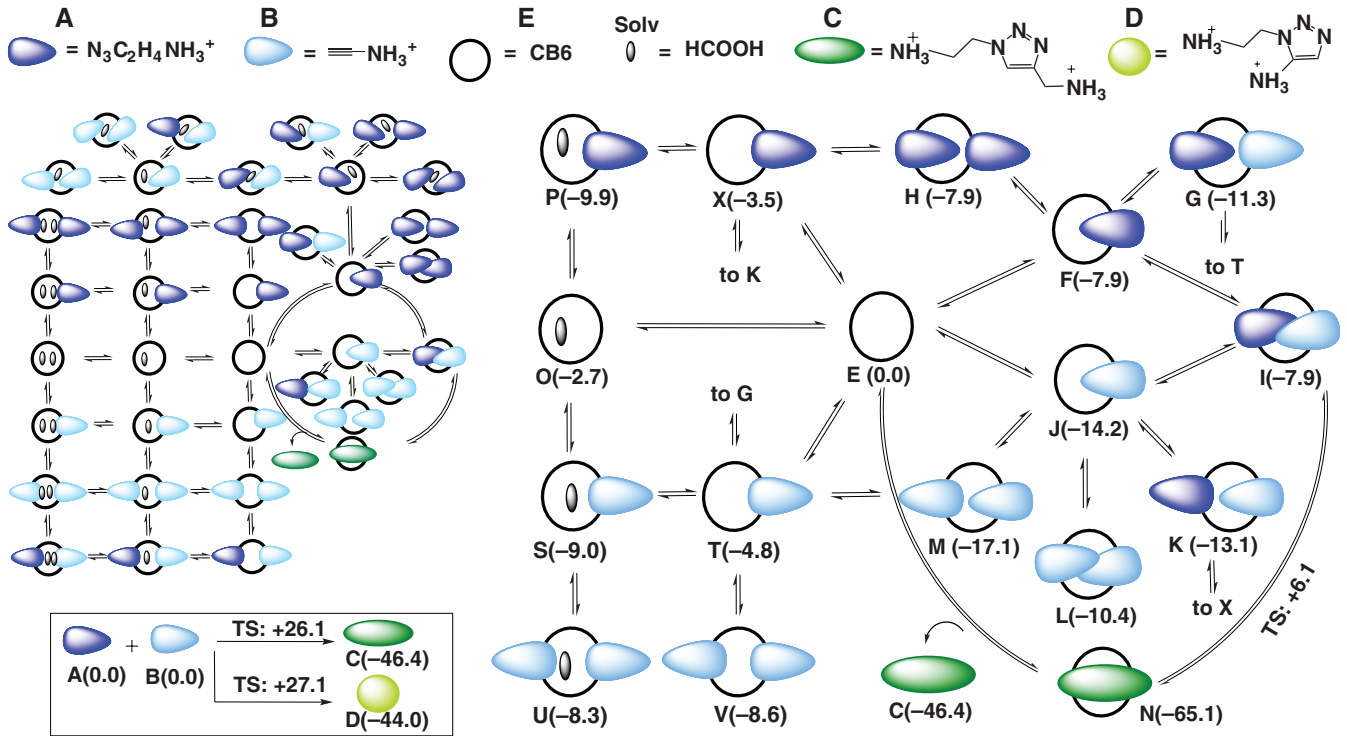

FIGURE 4 Top, legend of species representation. Right, reaction network of computed minima related to cucurbit[6]uril and its guests (some connections omitted). Left, pruned reaction network of structures selected for microkinetic model. Free energies in kcal/mol. Bottom left square, uncatalyzed reaction

ruled by the free energy difference from intermediate **J** (at −14.2 kcal/mol) to the transition state between **I** and **N** (at 6.1 kcal/mol). A barrier of 20.3 kcal/mol corresponds to the computed time for formation of **N** around 4 hr.

Direct inspection of free energies could have predicted that intermediate **M** should be formed, as it is the lowest adduct in the free energy surface, 2.9 kcal/mol lower than **J**. **M** corresponds to the coordination of a second alkyne molecule into **J**. Why is it that **M** is not the dominant species? The preference of **J** over **M** is related to concentration effects. The concentration of free alkyne in solution (3.75×10^{-3} M) is initially lower than that of the azide (1.5×10^{-2} M) and the solvent. Moreover, as the reaction proceeds and species **J** is formed the concentration of free alkyne goes much lower (about 8×10^{-4} M). We admit that these results could be deduced from a (very) careful analysis of the free energy profile, but the use of the microkinetic modeling provides them in a fast and elegant way.

Microkinetic modeling has been also applied to another system involving cucurbiturils, although in this case without reaction acceleration (Tootoonchi, Sharma, Calles, Prabhakar, & Kaifer, 2016). Also, recently we had used a similar approach to study the reaction network of a more complicated system. A cycloaddition reaction between neutral azide and alkyne inside a

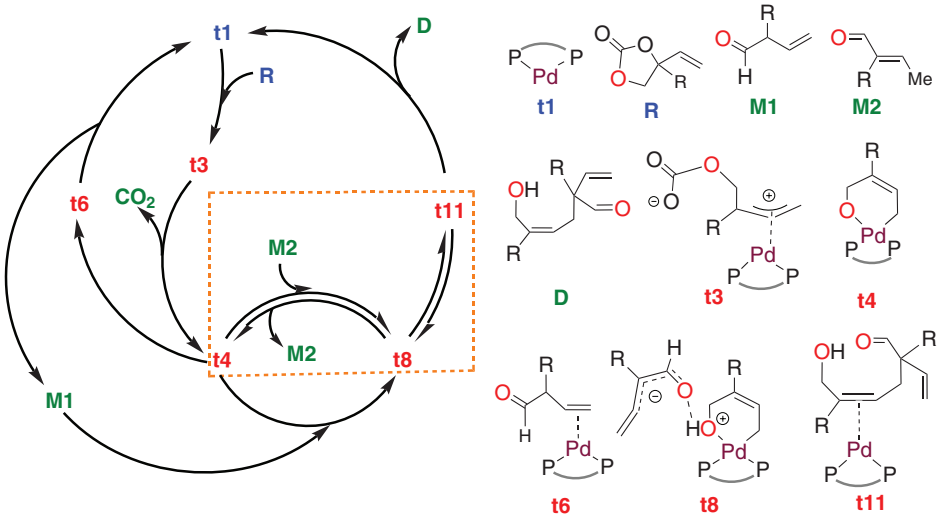

FIGURE 5 Schematic representation of the simplified mechanism for the Pd-catalyzed decarboxylative transformation of vinyl cyclic carbonates

self-assembled nanocapsule, a resorcinarene (Goehry, Besora, & Maseras, 2018). In this case, the reaction network is also very complex and microkinetic modeling is mandatory to reproduce the chemistry observed inside the nanocapsule.

3.3 | Interconnected catalytic cycles

A different type of complexity is the presence of different catalytic cycles sharing one or several intermediates. An example of application of microkinetic modeling to this type of processes is our study on the Pd-catalyzed decarboxylative transformation of vinyl cyclic carbonates (Guo et al., 2018). A simplified version of the catalytic cycle is shown in Figure 5. The reaction starts with catalyst **t1** and reactant **R** and results in the formation of two possible products, one of monomeric nature, **M2**, and another of dimeric nature, **D**. There is a first catalytic cycle, through intermediates **t1**, **t3**, **t4,** and **t6** that results in the production of aldehyde **M1**, which is later consumed inside the process. A second catalytic cycle is defined by intermediates **t1**, **t3**, **t4**, **t8,** and **t11**. This second cycle results in the irreversible formation of product **D**, and has as peculiarity the incorporation of species **M1** through interaction with **t4**. Thus, the second catalytic cycle cannot start until at least some amount of **M1** has been generated by the first cycle. The process is further complicated by the presence of an equilibrium between intermediates **t4** and **t8** that leads to the loss of aldehyde **M2**, which is an isomer of **M1** but is sufficiently stable to exist as final product.

The presence of three interlocked catalytic cycles, sharing some intermediates and with the presence of species **M1** being produced by one cycle and consumed by another one makes the analysis of the free energy profile of the system extremely complicated. It is very difficult to predict the approximate concentrations of the intermediates from the values of the free energies and understand the reactivity of the system. So, a microkinetic model is indeed necessary. The computational mechanism and energies together with the microkinetic model reproduce satisfactorily the experimental results (**D**:**M2** ratio; computational, 88:12; experimental, 90:10). Further analysis of the microkinetic model shows that the key is the equilibrium that takes place between the boxed species in Figure 5. And the key to decide the product ratios is in the competition between the exit channels of this equilibrium. One exit channel goes from **t11** to **t1** and leads to release of **D**. The other exit channel goes from **t4** to **t6**, and requires release of **M2**.

Another clear example of application of microkinetic models to interconnected catalytic cycles was reported by Kalek and Himo (2017). They studied the reaction between allylic carbonates and propargylic alcohols mediated by vanadium and palladium catalysts. The mechanism they propose combine five catalytic cycles involving different active species. Microkinetic models have been also applied to other systems of similar type, albeit with less complications. Jaraíz et al. (2017) studied the opening of epoxides by titanocene catalysts. The catalytic cycle is affected by the side reactions that deactivate the catalyst, and also by the concentration of the additives preventing this deactivation. Jover (2017) also used this approach in the study of the copper-catalyzed pentafluorination of benzoic acid chlorides through two different competing reaction pathways.

3.4 | Key species present in very low concentration

Inspection of free energies is sufficient for the interpretation of a chemical process when species in kinetically relevant reaction steps are in similar concentrations, within one order of magnitude. But concentration effects have to be taken into account

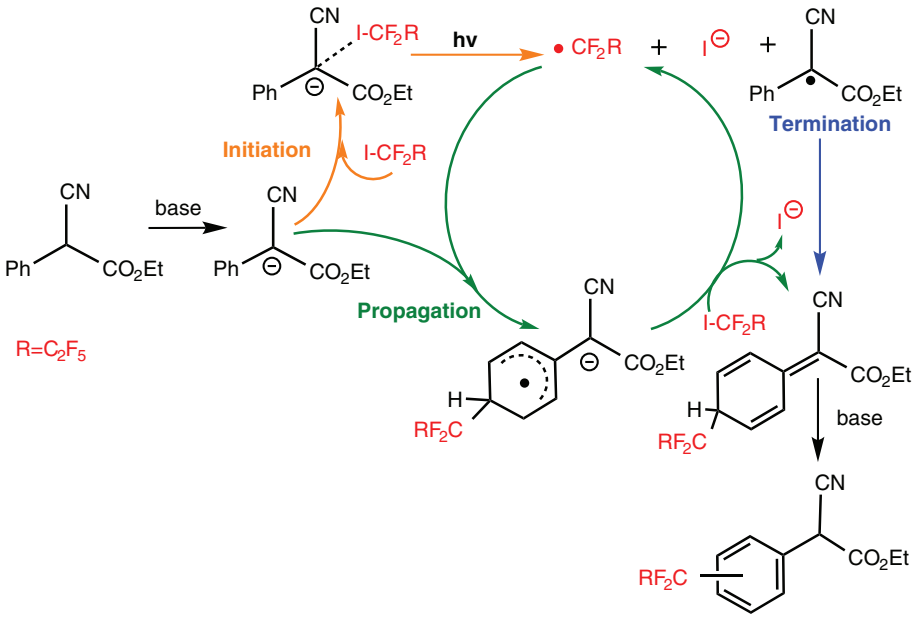

FIGURE 6 Schematic representation of the mechanism for the photo-initiated aromatic perfluoroalkylation of α-cyano arylacetates

when the difference in concentrations is larger than that. Because of this, microkinetic modeling is especially convenient when one of the key species is in very low concentration. This case is not at all unusual. The species resulting from excitation in photochemical reactions are in very low concentrations, as hydronium or hydroxyl ions in some acid–base reactions. Concentrations are also low for gases in solution, and they can be kept low by slow addition of one of the reactants in specific cases.

We discuss here an example of a photochemical reaction where microkinetic modeling plays a key role for the correct reproduction of the experimental results. The studied mechanism is the metal-free aromatic perfluoroalkylation of α-cyano arylacetates, that is photoinitiated by the irradiation of I-CF_2R (R = C_2F_5) under a fluorescent light in the presence of a base. The DFT mechanistic study resulted in the postulation of the reaction mechanism presented in Figure 6 (Fernández-Álvarez et al., 2015). The reaction starts by the deprotonation of the α-cyano arylacetate by the base. This anionic $[C(Ph)(CN)(COOEt)]^-$ species, path A, can interact with I-CF_2R to form an adduct that can be activated by a photon. Photoexcitation of this results in three species: the I^- anion and two radicals, $CF_2R^{\cdot}$ and $C(Ph)(CN)(COOEt)^{\cdot}$. The $CF_2R^{\cdot}$ radical can follow two different paths. One of them is a propagation pathway by reacting with a new molecule of the initial anion $[C(Ph)(CN)(COOEt)]^-$, which will lead to release of product and regeneration of the radical. The alternative is the termination path, through reaction with $C(Ph)(CN)(COOEt)^{\cdot}$. Interestingly, the propagation/termination dichotomy can be experimentally monitored by measurement of the quantum yield, the number of product molecules obtained per photon absorbed. The observed quantum yield is 4, which requires propagation to be competitive.

The computational study shows that the rate constant for propagation, k_{prop} (barrier-less in potential energy, diffusion-controlled), is much lower than that for termination, k_{term} ($\Delta G^{\ddagger}$ = 11.2 kcal/mol). But reaction rates depend also on concentrations, the propagation rate is equal to $k_{prop}[CF_2R^{\cdot}][C(Ph)(CN)(COOEt)^-]$, and the termination rate is equal to $k_{term}[CF_2R^{\cdot}][C(Ph)(CN)(COOEt)^{\cdot}]$ product. The concentration of $[C(Ph)(CN)(COOEt)]^-$ is much larger than that of the photochemically generated $C(Ph)(CN)(COOEt)^{\cdot}$. Introduction of the data in a microkinetic model takes into account properly the differences, and produces results in agreement with the experimental observation.

Another example that combines complex catalytic cycles and small concentration effects was reported by Harvey and coworkers (Rush et al., 2014). They studied a cobalt-catalyzed hydroformylation and found that the turnover was limited by the addition of the alkene to the active species. This step does not have a potential energy barrier but as the concentration of active species is very low (most of the cobalt is in form of unreactive dimer), the process is very slow. They also carried out simulations to rationalize the effect of the pressure of CO and H_2 on the reaction outcome. The study of Clot and coworkers on the Pd-catalyzed activation of intramolecular C—H bonds (Kefalidis et al., 2014) is also relevant. The authors studied the selectivity for the formation of benzocylobutene or olefin formation. Computational barriers alone postulate preference for the formation of benzocyclobutene products, but a microkinetic model is used to rationalize the experimental outcome. The key is in the dissociation of HCO_3^- formed after the C—H activation step. They performed simulations at different dissociation rates, showing their crucial effect in the reaction selectivity. In other words, the concentration of the intermediate HCO_3^- present along the reaction affects the reaction outcome. More recently, Clot and coworkers revealed the effect of the acetophenone/H_2 ratio in the hydrogenation of carbonyl derivatives with rhenium catalysts (Wei et al., 2017).

3.5 | Key species present in very high concentration

The counterpart to those described in the previous section is the case where one of the key species, usually the solvent acting as a reactant, is in a much higher concentration than the rest. We present here an example of this situation on a study on the reaction of aryl halides with the nickel complex $[Ni(PMe_nPh_{[3-n]})_4]$. The system shows competition of two reactions: halide abstraction and oxidative addition (Funes-Ardoiz et al., 2017). The mechanism for these two processes is presented in Figure 7. For PR_3 = PMe_3, the barriers for the oxidative addition were computed to be 14.9, 15.0, and 16.2 kcal/mol for PhCl, PhBr, and PhI, respectively, while for the halogen abstraction they were found to be 21.4, 16.3, and 10.0 kcal/mol for PhCl, PhBr, and PhI, respectively. Inspection of these barriers indicates that for PhCl, the oxidative addition should be largely

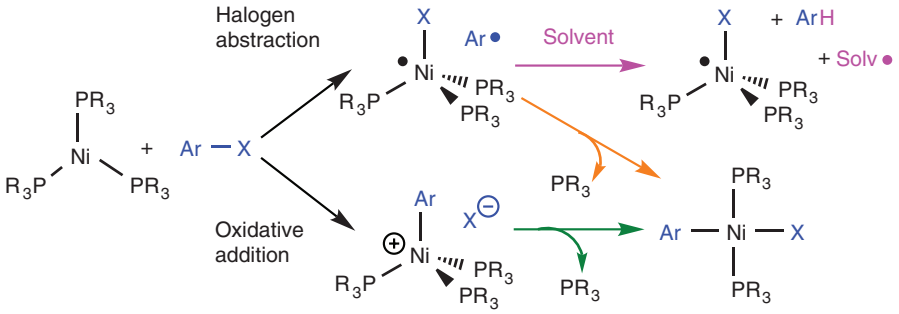

FIGURE 7 Schematic representation of the mechanism for the halogen abstraction (top) and oxidative addition (bottom)

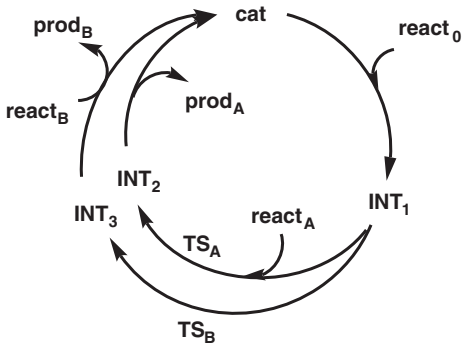

FIGURE 8 Examples of a hypothetical catalytic cycle highlighting the importance of reactions orders

preferred over the halogen abstraction, for PhI on the contrary the halogen abstraction has a much lower barrier. PhBr is in between with barriers differing only in 1.3 kcal/mol. Application of a Boltzmann distribution of products connected to the computed barriers would predict a computational selectivity of 0:100 for PhCl, 10:90 for PhBr, and 100:0 for PhI. However, the experimental values for this reaction do not fully agree, with values of 0:100, 19:81, and 80:20, respectively. In particular, the 80:20 selectivity for PhI is clearly at odds with a difference in energy barrier of 6.2 kcal/mol. The reason of the discrepancies is based on the behavior of the phenyl radical generated by the halogen abstraction. As it can be seen in Figure 7, this phenyl radical may still lead to the Ni(II) product of oxidative addition by association with the Ni(I) complex. The only way for the Ni(I) radical complex to remain in the media is that the phenyl radical reacts irreversibly with a solvent molecule. So the competition between the two reactions of Ph$^{\cdot}$ (purple and orange in Figure 7) becomes critical for the overall selectivity. The reaction with toluene has a barrier of 10.6 kcal/mol, while the reaction with $[NiX(PMe_3)_2]^{\cdot}$ is barrier-less, and is thus diffusion-controlled. This would suggest exclusive formation of the Ni(II) product, but the microkinetic modeling is able to account for the large difference in concentrations between toluene and the Ni(I) complexes, leading to a satisfactory reproduction of the experimental results. The final predicted values are 0:100 for PhCl, 8:92 for PhBr, and 83:17 for PhI.

3.6 | Unimolecular versus bimolecular steps

A less obvious example of counterintuitive chemoselectivity is supplied by the cases where the competition is between unimolecular and bimolecular steps. We have not found any clear example of this behavior, so we will present it with the generic example outlined in Figure 8. Two products can be formed through two catalytic cycles sharing some steps. One product, $prod_A$, is obtained from the reaction of $react_0$ and $react_A$, in a cycle where the highest barrier, through TS_A, takes place in the step where $react_B$ enters the cycle. The alternative product, $prod_B$, is obtained from the reaction of $react_0$ and $react_B$, in a cycle where the highest barrier, through TS_B, takes place before $react_B$ enters the catalytic cycle. Consequently, TS_A will have a second-order dependence on the concentration of $[INT_1][react_A]$ and TS_B a first order on $[INT_1]$. The concentration of $[INT_1]$ is the same for both processes. If we also assume similar rate constants for both steps, then the difference is only in the reaction order. This can seem a rather subtle issue, but it is not. In this example if we use equal barriers of 15.0 kcal/mol for TS_A and TS_B, and $[react_A]_0 = [react_B]_0 = 0.5$ M, at the end of the reaction we will get a 0.35 M of $prod_B$ and only a 0.15 M of $prod_A$. So reaction order matters. At lower concentrations of reactants, the difference in the amount of each product increases as the product with rate limiting step showing a first-order dependence is favored. For instance, if the initial concentrations are 10^{-2} M, the ratio of final products will be 99:1 in favor of $prod_B$. When the concentration increases, the amount of $prod_A$ increases. To have a 50% of each product we need to go up to $[react_A]_0 = [react_B]_0 \simeq 1.4$ M. At higher concentrations, the product with second-order dependence on the concentration of reactants will be favored. In Figure 9, a representation of the

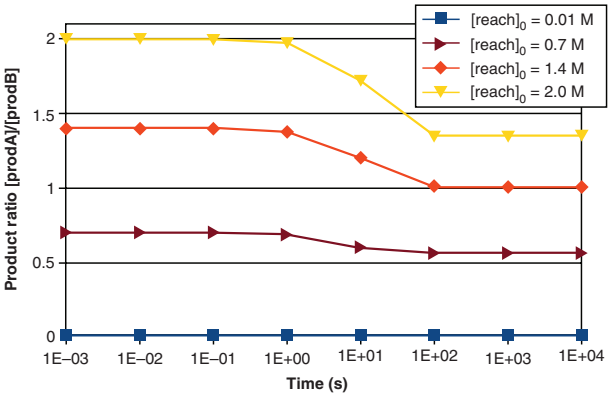

FIGURE 9 Evolution of the product ratio $[prod_A]/[prod_B]$ over time (in logarithmic scale and in seconds) in the hypothetic catalytic cycle. Four different sets of initial concentrations are considered: $[react_A]_0 = [react_B]_0 = 0.01$ M (blue), 0.7 M (brown), 1.4 M (orange), and 2.0 M (yellow)

evolution of the product ratio over time is presented for four different initial concentrations. In this plot we can observe that for initial concentrations $[react_A]_0 = [react_B]_0$ below 1.4 M, the formation of $prod_B$ is preferred, while for initial concentrations above 1.4 M, $prod_A$ is preferred. Please note that the product ratio changes along the reaction time because the concentrations of the reactants change as they are consumed.

4 | PRACTICAL ASPECTS

The application of microkinetic modeling to computational homogeneous catalysis involves little computational effort, but some aspects require some attention by the researcher. We will review some of them in this section, starting with two issues concerning the calculation of the rate constant.

For first-order elementary steps, the rate constant has units of reciprocal time, often s^{-1}. The rate constant comes directly from the application of the Eyring–Polanyi equation with the corresponding $\Delta G^{\ddagger}$, and no special care is required when taking directly the values resulting from application of a quantum chemistry code. Second-order elementary steps are trickier as the rate constant units have an additional dependence on reciprocal concentration, usually M^{-1}. In this case, the units for the rate constant derived from the Eyring–Polanyi equation will depend on the reference state that has been used in the calculation of $\Delta G^{\ddagger}$. Unfortunately, the free energy values supplied by most quantum chemistry programs do not use 1 M as reference state, but the concentration of an ideal gas at 298.15 K and 1 atm. If we want to have concentrations in M in our rate constant, we have to change the reference state. Luckily, this can be done by simply increasing the barrier by 1.89 kcal/mol if the temperature of the process is 298.15 K. There is strictly no requirement to use the 1 M reference state, and a consistent system could be deviced with a different reference state and different units for the rate constants. In particular, the standard state for some species, such as a reacting solvent, is not 1 M. However, we advice placing all free energies with respect to the 1 M reference state.

A second issue is related to the treatment of reactions that do not have a barrier on the potential energy surface. These are usually association/dissociation processes. They are not a problem when evaluating the feasibility of a mechanism, which they obviously do not hinder, but are a complication for kinetic models, where each single step must have a rate constant. Although these reactions are often referred as barrier-less, they do actually have a free energy barrier due to the loss of degrees of freedom and/or due to diffusion effects. If the barrier has a purely entropic nature, it can be estimated by scanning the potential energy surface and performing frequency calculations at each point (Besora et al., 2009). The maximum on the free energy could estimate the barrier the process. If the process is under diffusion control, a simple way to account for them is the use of Stokes–Einstein equation with the Smoluchowski relation. This means that the diffusion rate constant k_D can be approximated as $k_D = 8k_BT/3\eta$, where k_B is the Boltzmann constant, T is the temperature and η is the fluid viscosity (Rush et al., 2014). The practical barriers associated to each of these two phenomena are usually in the range of 3–4 kcal/mol. They are indeed low, but they can be critical as shown in some of the examples reported above.

Once we have written down all chemical equations with the corresponding rate constants, we can either write a script to solve the corresponding differential equations or use one of the many available software packages designed for this purpose. The advantage of using specialized software is saving the time-consuming and potentially error-prone step of programming, although it may limit flexibility. These software packages use as input chemical equations, rate constants and initial concentrations (plus other technical parameters as time step), and yield as output the evolution of the concentration of all species over time. We can mention three free software tools that we have used in our group: AChem (Braun, Herron, & Kahaner, 1988), Tenua (Wachsstock, 2007), and Copasi (Hoops et al., 2006). All three are very easy to use and reliable. The Tenua package is very easy to set-up, though it can get slow for complicated mechanisms. Copasi is fast, offers different mathematical options for the solution of the system of equations, and has versions for different operating systems including Linux. As weak points, the set-up may be rather slow for new users. Achem is fast and easy to set-up, but it has lesser options than Copasi. It does not provide graphical output, though it supplies the data to generate it.

It must also be acknowledged that microkinetic modeling will not correct mistakes in computed free energies. Computation gives errors and microkinetic models are in principle very sensitive to such errors. Where two competing steps are similar in structure, error cancellation may be favorable. But when comparing a unimolecular and a bimolecular step, for instance, error cancellation is unlikely to be perfect or even all that good. This can cause a "raw" microkinetic model to yield very incorrect numerical predictions. Results have to be always critically examined.

A final point we want to mention concerns the post-processing of the results of the microkinetic modeling. The main output is often a plot with the evolution of the concentrations of species over time. If the concentration of the species involved is very different it will be very difficult to represent in one graphic. This is quite common in catalysis as reactants have usually initial concentrations orders of magnitude higher than the catalysts. We have found that in some cases it might be a good idea to represent the axis of the concentration in logarithmic scale. With logarithmic scale we will be able to see in a graphic all the species, the logarithm can also be applied to time, if we need to show what happens in very short and very long reaction times.

This can be very convenient as reactions with rather high barriers might have interesting chemistry before the first second of the reaction (i.e., 10^{-5}-10^{-3} s), but do not yield products until a time scale of hours (10^{3}-10^{4} s) or days (10^{4}-10^{5} s).

5 | CONCLUSIONS

Microkinetic modeling is a useful technique that has found success in computational heterogeneous catalysis and experimental biochemistry, and seems now primed to make a significant contribution in computational homogeneous catalysis. Microkinetic models are simple to apply, demand little computational effort and constitute an excellent complement to the free energy profiles which are routinely computed nowadays with medium to high accuracy with DFT methods. They do not replace DFT calculations, which are indeed the usual source for the rate constants that are input in the model, but they introduce a new dimension concerning concentration effects that has been traditionally neglected but can be critical.

There are a lot of systems in homogeneous catalysis where microkinetic models can be relevant and there are some where its application, either direct or indirect, is mandatory for the reproduction/prediction of the chemistry that takes place in the experimental bench. We have outlined in this review the type of systems where this type of treatment has been shown to be critical, and illustrated their application with representative examples. A first block of systems consists of those with complex reaction networks. On one hand, the complexity can be associated to the sheer size of the network. The systems involved in host–guest catalysis present a large series of simultaneous equilibria where there is a coexistence of species necessary for the productive process, others interfering with it, and others which are not relevant. It is difficult to identify the key species from simple inspection of relative free energies. In contrast, the kinetic model provides directly the list of species with higher concentrations. The complexity may also be related to the topology of the reaction network. The presence of interlinked catalytic cycles, sharing intermediates that can be produced in one cycle and consumed in another poses a problem to conventional analysis techniques. It is difficult to ascertain the rate of steps where these intermediates are involved. A second block of systems where microkinetic modeling is recommended is defined by systems where a key species has concentrations that differ in orders of magnitude from the rest. Extremely low concentrations are present in a number of relatively usual cases, such as photocatalysis, acid–base chemistry or gas molecules dissolved in solution. Extremely large concentrations can also appear when the solvent participates as a key reactant in the system. If these species with very different concentrations are involved in any kinetically relevant step, microkinetic models may be useful, and they become mandatory when one of these kinetic steps is in a selectivity-deciding competition. There may well be other cases in homogeneous catalysis where microkinetic modeling is relevant but no examples are yet available. We have mentioned also in this review the potential of cases where unimolecular and bimolecular selectivity-determining steps are competing. It is important to remark that even in cases where microkinetic modeling happens to be not relevant, its performance will demand little effort and confirm the validity of more simple analysis.

Microkinetic models have been so far used mostly as a method to refine the information usually extracted from computed free energy profiles. In this sense, it has led to an improved prediction of reaction times and selectivities for a number of reactions. There is the potential for additional applications that remain so far relatively unexplored. On the one hand, microkinetic modeling opens new possibilities on the analysis of more raw experimental data involving the direct evolution of concentrations through time. A better comparison can be carried now with these experimental data, which can lead to a strengthened collaboration with experimental researchers. On the other hand, the performance of microkinetic modeling opens the path to low-cost high-value computational experiments. Computational affordable tests can be carried out to evaluate the role of changes of the initial concentrations, the reaction times or temperature. More elaborate analysis can be carried out on the role that the suppression of a given side reaction or additive would have in the overall behavior.

In summary, we hope to have demonstrated that microkinetic modeling is already a powerful tool for computational homogeneous catalysis. We foresee an extended application of this technique in the field in the near future.

ACKNOWLEDGMENTS

We thank MINECO grant CTQ2017-87792-R, Severo Ochoa Excellence Accreditation 2014–2018 SEV-2013-0319 and the CERCA Programme (Generalitat de Catalunya) for financial support.

CONFLICT OF INTEREST

The authors have declared no conflicts of interest for this article.

ORCID

Maria Besora http://orcid.org/0000-0002-6656-5827

REFERENCES

Aullón, G., Crespo, M., Font-Bardia, M., Jover, J., Martínez, M., & Pike, J. (2015). A combined kinetico-mechanistic and computational study on the competitive formation of seven- versus five-membered platinacycles; the relevance of spectator halide ligands. *Dalton Transactions*, *44*, 17968–17979. https://doi.org/10.1039/c5dt02657a

Balcells, D., & Maseras, F. (2007). Computational approaches to asymmetric synthesis. *New Journal of Chemistry*, *31*, 333–343. https://doi.org/10.1039/b615528f

Besora, M., Braga, A. A. C., Sameera, W. M. C., Urbano, J., Fructos, M. R., Pérez, P. J., & Maseras, F. (2015). A computational view on the reactions of hydrocarbons with coinage metal complexes. *Journal of Organometallic Chemistry*, *784*, 2–12. https://doi.org/10.1016/j.jorganchem.2014.10.009

Besora, M., Carreon-Macedo, J.-L., Cowan, A. J., George, M. W., Harvey, J. N., Portius, P., … Towrie, M. (2009). A combined theoretical and experimental study on the role of spin states in the chemistry of Fe(Co)(5) photoproducts. *Journal of the American Chemical Society*, *131*, 3583–3592. https://doi.org/10.1021/ja807149t

Besora, M., Vidossich, P., Lledós, A., Ujaque, G., & Maseras, F. (2018). Calculation of reaction free energies in solution: A comparison of current approaches. *Journal of Physical Chemistry A*, *122*, 1392–1399. https://doi.org/10.1021/acs.jpca.7b11580

Bligaard, T., Norskov, J. K., Dahl, S., Matthiesen, J., Christensen, C. H., & Sehested, J. (2004). The Bronsted–Evans–Polanyi relation and the volcano curve in heterogeneous catalysis. *Journal of Catalysis*, *224*, 206–217. https://doi.org/10.1016/j.jcat.2004.02.034

Braga, A. A. C., Caballero, A., Urbano, J., Diaz-Requejo, M. M., Pérez, P. J., & Maseras, F. (2011). Mechanism of side reactions in alkane C—H bond functionalization by diazo compounds catalyzed by Ag and Cu homoscorpionate complexes—a DFT study. *ChemCatChem*, *3*, 1646–1652. https://doi.org/10.1002/cctc.201100082

Braun, W., Herron, J. T., & Kahaner, D. K. (1988). Acuchem—a computer-program for modeling complex chemical-reaction systems. *International Journal of Chemical Kinetics*, *20*, 51–62. https://doi.org/10.1002/kin.550200107

Carpenter, B. K., Harvey, J. N., & Orr-Ewing, A. J. (2016). The study of reactive intermediates in condensed phases. *Journal of the American Chemical Society*, *138*, 4695–4705. https://doi.org/10.1021/jacs.6b01761

Chmely, S. C., Kim, S., Ciesielski, P. N., Jimenez-Oses, G., Paton, R. S., & Beckham, G. T. (2013). Mechanistic study of a Ru-Xantphos catalyst for tandem alcohol dehydrogenation and reductive aryl-ether cleavage. *ACS Catalysis*, *3*, 963–974. https://doi.org/10.1021/cs400110r

Colby, D. A., Bergman, R. G., & Ellman, J. A. (2008). Synthesis of dihydropyridines and pyridines from imines and alkynes via C—H activation. *Journal of the American Chemical Society*, *130*, 3645–3651. https://doi.org/10.1021/ja7104784

Corro, M., Besora, M., Maya, C., Alvarez, E., Urbano, J., Fructos, M. R., … Perez, P. J. (2014). Catalytic copper-mediated ring opening and functionalization of benzoxazoles. *ACS Catalysis*, *4*, 4215–4222. https://doi.org/10.1021/cs5012519

Dewyer, A. L., Arguelles, A. J., & Zimmerman, P. M. (2018). Methods for exploring reaction space in molecular systems. *WIREs Computational Molecular Science*, *8*, e1354. https://doi.org/10.1002/wcms.1354

Diao, T., & Stahl, S. S. (2011). Synthesis of cyclic enones via direct palladium-catalyzed aerobic dehydrogenation of ketones. *Journal of the American Chemical Society*, *133*, 14566–14569. https://doi.org/10.1021/ja206575j

Dumesic, J. A., Rudd, D. F., Aparicio, L. M., Rekoske, J. E., & Treviño, A. A. (1993). The microkinetics of heterogeneous catalysis. In J. A. Dumesic (Ed.), *ACS Professional Reference Book*. Washington, DC: American Chemical Society ISBN: 9780841222144.

Eyring, H. (1935). The activated complex in chemical reactions. *Journal of Chemical Physics*, *3*, 107–115. https://doi.org/10.1063/1.1749604

Fernández-Álvarez, V. M., Nappi, M., Melchiorre, P., & Maseras, F. (2015). Computational study with DFT and kinetic models on the mechanism of photoinitiated aromatic perfluoroalkylations. *Organic Letters*, *17*, 2676–2679. https://doi.org/10.1021/acs.orglett.5b01069

Fructos, M. R., Besora, M., Braga, A. A. C., Diaz-Requejo, M. M., Maseras, F., & Pérez, P. J. (2017). Mechanistic studies on gold-catalyzed direct arene C—H bond functionalization by carbene insertion: The coinage-metal effect. *Organometallics*, *36*, 172–179. https://doi.org/10.1021/acs.organomet.6b00604

Funes-Ardoiz, I., Nelson, D. J., & Maseras, F. (2017). Halide abstraction competes with oxidative addition in the reactions of aryl halides with [Ni(PMenPh(3-n))(4)]. *Chemistry—A European Journal*, *23*, 16728–16733. https://doi.org/10.1002/chem.201702331

Gava, R., Fuentes, M. A., Besora, M., Belderrain, T. R., Jacob, K., Maseras, F., … Perez, P. J. (2014). Silver-catalyzed functionalization of esters by carbene transfer: The role of ylide zwitterionic intermediates. *ChemCatChem*, *6*, 2206–2210. https://doi.org/10.1002/cctc.201402241

Goehry, C., Besora, M., & Maseras, F. (2015). Computational study on the mechanism of the acceleration of 1,3-dipolar cycloaddition inside cucurbit[6]uril. *ACS Catalysis*, *5*, 2445–2451. https://doi.org/10.1021/cs501703t

Goehry, C., Besora, M., & Maseras, F. (2018). Computational description of a huisgen cycloaddition inside a self-assembled nanocapsule. *European Journal of Organic Chemistry*. https://doi.org/10.1002/ejoc.201800179

Guo, W., Kuniyil, R., Gómez, J. E., Maseras, F., & Kleij, A. W. (2018). A domino process toward functionally dense quaternary carbons through Pd-catalyzed decarboxylative c(sp3)–c(sp3) bond formation. *Journal of the American Chemical Society.*, *140*, 3981–3987. https://doi.org/10.1021/jacs.7b12608

Hartenbach, A. E., Hofstetter, T. B., Aeschbacher, M., Sander, M., Kim, D., Strathmann, T. J., … Schwarzenbach, R. P. (2008). Variability of nitrogen isotope fractionation during the reduction of nitroaromatic compounds with dissolved reductants. *Environmental Science and Technology*, *42*, 8352–8359. https://doi.org/10.1021/es801063u

Herrgard, M. J., Swainston, N., Dobson, P., Dunn, W. B., Arga, K. Y., Arvas, M., … Kell, D. B. (2008). A consensus yeast metabolic network reconstruction obtained from a community approach to systems biology. *Nature Biotechnology*, *26*, 1155–1160. https://doi.org/10.1038/nbt1492

Hoops, S., Sahle, S., Gauges, R., Lee, C., Pahle, J., Simus, N., … Kummer, U. (2006). COPASI—a complex pathway simulator. *Bioinformatics*, *22*, 3067–3074. https://doi.org/10.1093/bioinformatics/btl485

Hopmann, K. H. (2015). Quantum chemical studies of asymmetric reactions: Historical aspects and recent examples. *International Journal of Quantum Chemistry*, *115*, 1232–1249. https://doi.org/10.1002/qua.24882

Jaraíz, M., Enriquez, L., Pinacho, R., Rubio, J. E., Lesarri, A., & López-Pérez, J. L. (2017). A DFT-based computational-experimental methodology for synthetic chemistry: Example of application to the catalytic opening of epoxides by titanocene. *Journal of Organic Chemistry*, *82*, 3760–3766. https://doi.org/10.1021/acs.joc.7b00220

Jensen, V. R., Koley, D., Jagadeesh, M. N., & Thiel, W. (2005). DFT investigation of the single-center, two-state model for the broken rate order of transition metal catalyzed olefin polymerization. *Macromolecules*, *38*, 10266–10278. https://doi.org/10.1021/ma051224a

Jover, J. (2017). Quantitative DFT modeling of product concentration in organometallic reactions: Cu-mediated pentafluoroethylation of benzoic acid chlorides as a case study. *Physical Chemistry Chemical Physics*, *19*, 29344–29353. https://doi.org/10.1039/c7cp05709a

Kalek, M., & Himo, F. (2017). Mechanism and selectivity of cooperatively catalyzed Meyer–Schuster rearrangement/Tsuji–Trost allylic substitution. Evaluation of synergistic catalysis by means of combined DFT and kinetics simulations. *Journal of the American Chemical Society*, *139*, 10250–10266. https://doi.org/10.1021/jacs.7b01931

Kefalidis, C. E., Davi, M., Holstein, P. M., Clot, E., & Baudoin, O. (2014). Mechanistic study of the selectivity of olefin versus cyclobutene formation by palladium (0)-catalyzed intramolecular C(sp(3))—H activation. *Journal of Organic Chemistry*, *79*, 11903–11910. https://doi.org/10.1021/jo501610x

Kelly, C. P., Cramer, C. J., & Truhlar, D. G. (2006). Aqueous solvation free energies of ions and ion-water clusters based on an accurate value for the absolute aqueous solvation free energy of the proton. *Journal of Physical Chemistry B*, *110*, 16066–16081. https://doi.org/10.1021/jp063552y

Kim, Y., Kim, J. W., Kim, Z., & Kim, W. Y. (2018). Efficient prediction of reaction paths through molecular graph and reaction network analysis. *Chemical Science*, *9*, 825–835. https://doi.org/10.1039/c7sc03628k

Kozuch, S., & Shaik, S. (2011). How to conceptualize catalytic cycles? The energetic span model. *Accounts of Chemical Research*, *44*, 101–110. https://doi.org/10.1021/ar1000956

Mao, Y., Wang, H. F., & Hu, P. (2017). Theory and applications of surface micro-kinetics in the rational design of catalysts using density functional theory calculations. *WIREs Computational Molecular Science*, *7*, e1321. https://doi.org/10.1002/wcms.1321

Martinez-Nuñez, E. (2015). An automated method to find transition states using chemical dynamics simulations. *Journal of Computational Chemistry*, *36*, 222–234. https://doi.org/10.1002/jcc.23790

Michalak, A., & Ziegler, T. (2002). Stochastic simulations of polymer growth and isomerization in the polymerization of propylene catalyzed by Pd-based diimine catalysts. *Journal of the American Chemical Society*, *124*, 7519–7528. https://doi.org/10.1021/ja012144z

Michalak, A., & Ziegler, T. (2003). Polymerization of ethylene catalyzed by a nickel(+2) anilinotropone-based catalyst: DFT and stochastic studies on the elementary reactions and the mechanism of polyethylene branching. *Organometallics*, *22*, 2069–2079. https://doi.org/10.1021/om030072+

Miranda, M. O., DePorre, Y., Vazquez-Lima, H., Johnson, M. A., Marell, D. J., Cramer, C. J., & Tolman, W. B. (2013). Understanding the mechanism of polymerization of epsilon-caprolactone catalyzed by aluminum salen complexes. *Inorganic Chemistry*, *52*, 13692–13701. https://doi.org/10.1021/ic402255m

Muñoz-Molina, J. M., Sameera, W. M. C., Álvarez, E., Maseras, F., Belderrain, T. R., & Pérez, P. J. (2011). Mechanistic and computational studies of the atom transfer radical addition of CCl4 to styrene catalyzed by copper homoscorpionate complexes. *Inorganic Chemistry*, *50*, 2458–2467. https://doi.org/10.1021/ic102279w

Olson, E. J., Isley, W. C., Brennan, J. E., Cramer, C. J., & Buehlmann, P. (2015). Electrochemical reduction of 2,4-dinitrotoluene in aprotic and pH-buffered media. *Journal of Physical Chemistry C*, *119*, 13088–13097. https://doi.org/10.1021/acs.jpcc.5b02840

Rush, L. E., Pringle, P. G., & Harvey, J. N. (2014). Computational kinetics of cobalt-catalyzed alkene hydroformylation. *Angewandte Chemie, International Edition*, *53*, 8672–8676. https://doi.org/10.1002/anie.201402115

Sameera, W. M. C., Maeda, S., & Morokuma, K. (2016). Computational catalysis using the artificial force induced reaction method. *Accounts of Chemical Research*, *49*, 763–773. https://doi.org/10.1021/acs.accounts.6b00023

Sameera, W. M. C., & Maseras, F. (2012). Transition metal catalysis by density functional theory and density functional theory/molecular mechanics. *WIREs Computational Molecular Science*, *2*, 375–385. https://doi.org/10.1002/wcms.1092

Santoro, S., Kalek, M., Huang, G., & Himo, F. (2016). Elucidation of mechanisms and selectivities of metal-catalyzed reactions using quantum chemical methodology. *Accounts of Chemical Research*, *49*, 1006–1018. https://doi.org/10.1021/acs.accounts.6b00050

Slusarczyk, A. L., Lin, A., & Weiss, R. (2012). Foundations for the design and implementation of synthetic genetic circuits. *Nature Reviews. Genetics*, *13*, 406–420. https://doi.org/10.1038/nrg3227

Sperger, T., Fisher, H. C., & Schoenebeck, F. (2016). Computationally deciphering palladium-catalyzed reaction mechanisms. *WIREs Computational Molecular Science*, *6*, 226–242. https://doi.org/10.1002/wcms.1244

Thiel, W. (2014). Computational catalysis—past, present, and future. *Angewandte Chemie, International Edition*, *53*, 8605–8613. https://doi.org/10.1002/anie.201402118

Tootoonchi, M. H., Sharma, G., Calles, J., Prabhakar, R., & Kaifer, A. E. (2016). Cooperative self-assembly of a quaternary complex formed by two cucurbit[7]uril hosts, cyclobis(paraquat-p-phenylene), and a "designer" guest. *Angewandte Chemie, International Edition*, *55*, 11507–11511. https://doi.org/10.1002/anie.201606038

Trinh, C. T., Wlaschin, A., & Srienc, F. (2009). Elementary mode analysis: A useful metabolic pathway analysis tool for characterizing cellular metabolism. *Applied Microbiology and Biotechnology*, *81*, 813–826. https://doi.org/10.1007/s00253-008-1770-1

Wachsstock, D. (2007). Tenua: The kinetics simulator for java. Retrieved from http://bililite.com/tenua

Wei, D., Roisnel, T., Darcel, C., Clot, E., & Sortais, J. B. (2017). Hydrogenation of carbonyl derivatives with a well-defined rhenium precatalyst. *ChemCatChem*, *9*, 80–83. https://doi.org/10.1002/cctc.201601141

Winikoff, S. G., & Cramer, C. J. (2014). Mechanistic analysis of water oxidation catalyzed by mononuclear copper in aqueous bicarbonate solutions. *Catalysis Science & Technology*, *4*, 2484–2489. https://doi.org/10.1039/c4cy00500g

How to cite this article: Besora M, Maseras F. Microkinetic modeling in homogeneous catalysis. *WIREs Comput Mol Sci*. 2018;8:e1372. https://doi.org/10.1002/wcms.1372